Nonlinear Dynamics manuscript No.
(will be inserted by the editor)

Iterative Learning Control Based on Sliding Mode Technique for Hybrid Force/Position Control of Robot Manipulators

Xinxin Zhang · Huafeng Ding · Min Li · Andrés Kecskeméthy

Received: date / Accepted: date

Abstract In this paper, an iterative learning control (ILC) method based on sliding mode technique is proposed for hybrid force/position control of robot manipulators. Different from traditional ILC, the main purpose of the proposed ILC is to learn the dynamic parameters rather than the control signals. The sliding mode technique is applied to enhance the robustness of the proposed ILC method against external disturbances and noise. The switching gain of the sliding mode term is time-varying and learned by ILC such that the chattering is suppressed effectively compared to traditional sliding mode control (SMC). Simulation studies are performed on a two degrees of freedom planar parallel manipulator. Simulation results demonstrate that the proposed method can achieve higher force/position tracking performance than the traditional SMC and ILC.

Keywords Iterative learning control · hybrid force/position control · robot manipulators · sliding mode control

1 Introduction

In industrial applications, such as grinding, deburring, polishing, etc. [1–5], robot manipulators usually need to interact with the environment. During the interaction process, the motion of the end-effector of the robot manipulators is constrained by the environment. In this case, the contact force between the robot manipulators and the environment should be controlled. To deal with this problem, hybrid force/position control is investigated in recent years. The main idea of hybrid force/position control is to decompose the cartesian-space coordinates of the end-effector into a position subspace and a force subspace and then the position trajectory and force trajectory are tracked in the position subspace and force subspace, respectively. The early research of hybrid force/position control was in the 1980s [6, 7]. The concept of hybrid force/position control is first developed by Mason [6] and realized by Raibert [7]. Subsequently, more and more researchers focus on hybrid force/position control. A sliding mode control (SMC) method is proposed for force/position control of constrained robot manipulators with parametric uncertainties in [8]. Based on three kinds of sensors including encoder, force-torque sensor and visual sensor, a hybrid force/position control method is proposed for robot manipulators working in an uncalibrated environment by Xiao et al. [9]. A hybrid force/position control method is proposed for a parallel manipulator with a flexible link for contact task with the environment by Madani et al. [10]. Based on the computed torque method, Cazalilla et al. [11] design a real-time hybrid force/position controller for a three degrees of freedom (DOFs) parallel robot.

However, the aforementioned strategies all require the accurate system model of manipulators which is difficult to be obtained since the nonlinear, coupling and time-varying of the manipulators. To reduce the dependence on the accuracy of system model, fuzzy control [12–14], neural network (NN) methods [15–18], adaptive control [19–22], etc, and the combination of those

Xinxin Zhang · Huafeng Ding(✉) · Min Li
School of Mechanical Engineering and Electronic Information, China University of Geosciences (Wuhan), Wuhan 430074, P.R. China
E-mail: dinghf@cug.edu.cn

Xinxin Zhang · Andrés Kecskeméthy
Laboratory of Mechanics and Robotics, Faculty of Engineering, University of Duisburg-Essen, Duisburg, 47057, Germany
E-mail: zhangxx@cug.edu.cn

methods [23–25] are integrated with the force/position control to enhance the robustness against model uncertainties. By using singular perturbation approach, a hierarchical fuzzy logic controller is designed for hybrid force/position control of a flexible robot arm [12]. A fuzzy controller is proposed for force/position control of a rehabilitation robot by Ju et al. [13]. However, there is no systematic approach to design fuzzy rules and membership functions. Based on adaptive control, a feedforward NN which is employed to learn the parametric uncertainties of controlled system is integrated into hybrid force/position control for rigid robot manipulators [16]. Based on terminal sliding mode and NN, a force/position control method is proposed for manipulators to ensure the convergent performance without the nominal model of the system dynamics by Cao et al. [17]. However, NN control is limited in practice since it suffers from heavy computational effort. In [20], the unknown parameters of the robot and environment compliance are estimated along with the force control by adaptive estimators. In [21], a force/velocity observer and an adaptive force/position control law are combined for the force/position control of robot manipulators with the change of parameters. Furthermore, some mixed methods are developed for force/position control. For example, force/position control methods are proposed for robot manipulators based on adaptive fuzzy SMC by Karamali Ravandi et al. [23] and extended adaptive fuzzy SMC by Navvabi et al. [24]. In [25], based on adaptive neuro-fuzzy control, a hybrid force/position control method is proposed for an industrial robot manipulator.

Another promising method for force/position control of industrial robot manipulators is iterative learning control (ILC). ILC is a data-driven method that does not require the model information of controlled system [26, 27]. In general, ILC can realize perfect trajectory tracking performance for the cases that perform repetitive tasks over a finite time-interval [28, 29]. Since it is very common for manipulators to perform repetitive tasks in industrial applications, ILC is very suitable for the control of manipulators [30–32]. A position-based impedance control method combined with Newton-type ILC is proposed to achieve accurate force control for robot manipulators [33]. A force/position control method combined with the ILC is proposed for the robot to track high-speed force trajectories to reduce the force tracking error in [34]. An impedance control method combined with reinforcement learning procedure which is used to learn the friction parameters and damping ratio of the interacting environment is proposed for high accuracy force tracking by [35]. However, disturbances and noise are not taken into consideration in those papers which is inevitable in practical applications.

Motivated by the above observations, an ILC method based on sliding mode technique is proposed for hybrid force/position control of robot manipulators. The proposed ILC is used to learn the dynamic parameters of robot manipulators rather than the control signals. On the other hand, the sliding mode technique is integrated into the ILC method to enhance the robustness against external disturbances and noise. To suppress the chattering inducing by the sliding mode technique, the switching gain is designed to be time-varying and learned by ILC. Simulation studies are performed on a 2-DOFs planar parallel manipulator to confirm the proposed ILC method outperforms the tradition SMC and ILC.

The outline of this paper is as follows. In Section 2, the robot manipulator and the interacting environment are modeled. The proposed method is presented in Section 3. In Section 4, simulation studies are provided to demonstrate the effectiveness of the proposed method. Finally, the conclusions are given in Section 5.

Notations: $\mathbb{R}^n$ represents the n-dimensional Euclidean space. $\boldsymbol{I}$ and $\boldsymbol{0}$ denote the identity matrix and the zero matrix with property size, respectively. $[\boldsymbol{M}]_{ij}$ denotes the element of row i and column j of matrix $\boldsymbol{M}$.

2 Modeling of robot manipulator

Consider an n-DOFs robot manipulator, the equation of the dynamics model in joint space is given by [36]

$$\boldsymbol{D}_q(\boldsymbol{q}')\ddot{\boldsymbol{q}} + \boldsymbol{C}_q(\boldsymbol{q}', \dot{\boldsymbol{q}}')\dot{\boldsymbol{q}} + \boldsymbol{G}_q(\boldsymbol{q}) + \boldsymbol{\tau}_v = \boldsymbol{\tau} \tag{1}$$

where $\boldsymbol{q}'$ and $\boldsymbol{q}$ denote vectors of joint variables (angles for revolute joints and displacements for prismatic joints) and actuated joint variables. $\boldsymbol{D}_q(\boldsymbol{q}')$, $\boldsymbol{C}_q(\boldsymbol{q}', \dot{\boldsymbol{q}}')$ and $\boldsymbol{G}_q$ denote the inertia matrix, centripetal Coriolis matrix and the gravity vector of the robot manipulator, respectively. $\boldsymbol{\tau}$ and $\boldsymbol{\tau}_v$ represent vectors of actuated joint torques and external disturbances. Assume that $\boldsymbol{\tau}_v$ is bounded and satisfied that

$$\left\| \left(\boldsymbol{J}^T\right)^{-1} \boldsymbol{\tau}_v \right\| \leq b_v(t) = \alpha(t), \quad \forall t \in [0,\ T] \tag{2}$$

where $\boldsymbol{J}$ is the Jacobian matrix.

Since the interaction with environment is inevitable in hybrid force/position control, it is worth considering the dynamic model of the manipulator in task space. Equation (1) can be rewritten as

$$\boldsymbol{D}(\boldsymbol{q}')\ddot{\boldsymbol{P}} + \boldsymbol{C}(\boldsymbol{q}', \dot{\boldsymbol{q}}')\dot{\boldsymbol{P}} + \boldsymbol{G}(\boldsymbol{q}) + \boldsymbol{F}_v = \boldsymbol{F}_E \tag{3}$$

where $\dot{\boldsymbol{P}}$ and $\ddot{\boldsymbol{P}}$ denote the velocity and acceleration of the end-effector in task space. $\boldsymbol{F}_v$ and $\boldsymbol{F}_E$ denote the disturbance and force of the end-effector and can be calculated by $\boldsymbol{F}_v = \left(\boldsymbol{J}^T\right)^{-1}\boldsymbol{\tau}_v$ and $\boldsymbol{F}_E = \left(\boldsymbol{J}^T\right)^{-1}\boldsymbol{\tau}$. The inertia matrix, centripetal Coriolis matrix and the gravity vector are given as

$$\begin{cases} \boldsymbol{D}\left(\boldsymbol{q}'\right) = \left(\boldsymbol{J}^T\right)^{-1}\boldsymbol{D}_q\left(\boldsymbol{q}'\right)\boldsymbol{J}^{-1} \\ \boldsymbol{C}\left(\boldsymbol{q}', \dot{\boldsymbol{q}}'\right) = -\left(\boldsymbol{J}^T\right)^{-1}\boldsymbol{D}_q\left(\boldsymbol{q}'\right)\boldsymbol{J}^{-1}\dot{\boldsymbol{J}}\boldsymbol{J}^{-1} \\ \qquad\qquad + \left(\boldsymbol{J}^T\right)^{-1}\boldsymbol{C}_q\left(\boldsymbol{q}', \dot{\boldsymbol{q}}'\right)\boldsymbol{J}^{-1} \\ \boldsymbol{G}\left(\boldsymbol{q}\right) = \left(\boldsymbol{J}^T\right)^{-1}\boldsymbol{G}_q\left(\boldsymbol{q}\right) \end{cases}. \tag{4}$$

It is well known that robot manipulators have the following properties [36]:

P1: $\boldsymbol{D}\left(\boldsymbol{q}'\right)$ is a symmetric, bounded and positive definite matrix.

P2: The matrix $\dot{\boldsymbol{D}}\left(\boldsymbol{q}'\right) - 2\boldsymbol{C}\left(\boldsymbol{q}', \dot{\boldsymbol{q}}'\right)$ is skew symmetric, i.e.,

$$\boldsymbol{x}^T\left(\dot{\boldsymbol{D}}\left(\boldsymbol{q}'\right) - 2\boldsymbol{C}\left(\boldsymbol{q}', \dot{\boldsymbol{q}}'\right)\right)\boldsymbol{x} = 0 \qquad \forall \boldsymbol{x} \in \mathbb{R}^n. \tag{5}$$

3 ILC based on sliding mode technique for hybrid force/position control

In this section, an ILC method combined with SMC is proposed to improve the force and position tracking performance for robot manipulators.

3.1 Controller design

Firstly, a binary selection vector $\boldsymbol{s} \in \mathbb{R}^n$ is introduced to specify which DOFs are under force control and which DOFs are under position control. Define selection matrix $\boldsymbol{S} = \mathrm{diag}(\boldsymbol{s})$ and $\bar{\boldsymbol{S}} = \boldsymbol{I} - \boldsymbol{S}$.

The position tracking error $\boldsymbol{e}_P$ and force tracking error $\boldsymbol{e}_F$ are given as

$$\boldsymbol{e}_P(t) = \bar{\boldsymbol{S}}\left(\boldsymbol{P}_d(t) - \boldsymbol{P}(t)\right) \tag{6}$$

$$\boldsymbol{e}_F(t) = \boldsymbol{S}\left(\boldsymbol{F}_d(t) - \boldsymbol{F}(t)\right) \tag{7}$$

where $\boldsymbol{P}_d(t)$ and $\boldsymbol{P}(t)$ denote the desired reference and actual reference of the end-effector, $\boldsymbol{F}_d(t)$ and $\boldsymbol{F}(t)$ denote the desired contact force and the actual contact force between the end-effector and the environment, respectively.

For the considered system, a sliding surface is defined as

$$\begin{aligned} \boldsymbol{\sigma}(t) &= \boldsymbol{\sigma}_P(t) + \boldsymbol{\sigma}_F(t) \\ &= \boldsymbol{\lambda}_P\boldsymbol{e}_P(t) + \dot{\boldsymbol{e}}_P(t) + \boldsymbol{\lambda}_{F1}\boldsymbol{e}_F(t) + \boldsymbol{\lambda}_{F2}\dot{\boldsymbol{e}}_F(t) \end{aligned} \tag{8}$$

with $\boldsymbol{\lambda}_P$, $\boldsymbol{\lambda}_{F1}$ and $\boldsymbol{\lambda}_{F2}$ are diagram matrix. $[\lambda_P]_{ii}$, $[\lambda_{F1}]_{ii}$ and $[\lambda_{F2}]_{ii}$ are coefficients of a Hurwitz polynomial for $i = [1, 2, ..., n]$.

For simplicity, the argument t is omitted in the following formulas, and $\boldsymbol{D}\left(\boldsymbol{q}'\right)$, $\boldsymbol{C}\left(\boldsymbol{q}', \dot{\boldsymbol{q}}'\right)$ and $\boldsymbol{G}\left(\boldsymbol{q}\right)$ are denoted as $\boldsymbol{D}$, $\boldsymbol{C}$ and $\boldsymbol{G}$.

Taking derivatives with respect to time t on both sides of (8), we can obtain

$$\begin{aligned} \dot{\boldsymbol{\sigma}} =& \dot{\boldsymbol{\sigma}_P} + \dot{\boldsymbol{\sigma}_F} \\ =& \boldsymbol{\lambda}_P\dot{\boldsymbol{e}}_P + \ddot{\boldsymbol{e}}_P + \boldsymbol{\lambda}_{F1}\dot{\boldsymbol{e}}_F + \boldsymbol{\lambda}_{F2}\ddot{\boldsymbol{e}}_F \\ =& \boldsymbol{\lambda}_P\dot{\boldsymbol{e}}_P + \boldsymbol{\lambda}_{F1}\dot{\boldsymbol{e}}_F + \boldsymbol{\lambda}_{F2}\ddot{\boldsymbol{e}}_F + \bar{\boldsymbol{S}}\ddot{\boldsymbol{P}}_d - \bar{\boldsymbol{S}}\ddot{\boldsymbol{P}} \\ =& \boldsymbol{\lambda}_P\dot{\boldsymbol{e}}_P + \boldsymbol{\lambda}_{F1}\dot{\boldsymbol{e}}_F + \boldsymbol{\lambda}_{F2}\ddot{\boldsymbol{e}}_F + \bar{\boldsymbol{S}}\ddot{\boldsymbol{P}}_d + \boldsymbol{S}\ddot{\boldsymbol{P}}(t) - \ddot{\boldsymbol{P}} \\ =& \boldsymbol{\lambda}_P\dot{\boldsymbol{e}}_P + \boldsymbol{\lambda}_{F1}\dot{\boldsymbol{e}}_F + \boldsymbol{\lambda}_{F2}\ddot{\boldsymbol{e}}_F + \bar{\boldsymbol{S}}\ddot{\boldsymbol{P}}_d + \boldsymbol{S}\ddot{\boldsymbol{P}} \\ & - \boldsymbol{D}^{-1}\left(\left(\boldsymbol{J}^T\right)^{-1}\boldsymbol{\tau} - \boldsymbol{F}_v - \boldsymbol{C}\dot{\boldsymbol{P}} - \boldsymbol{G} + \boldsymbol{F}\right). \end{aligned} \tag{9}$$

Design a Lyapunov function at j-th iteration as

$$E_j = \frac{\boldsymbol{\sigma}_j^T\boldsymbol{D}\boldsymbol{\sigma}_j}{2}. \tag{10}$$

Then, by using the property **P1** and (3), the derivative of E_j is derived as

$$\begin{aligned} \dot{E}_j =& \boldsymbol{\sigma}_j^T\boldsymbol{D}\dot{\boldsymbol{\sigma}}_j + \frac{\boldsymbol{\sigma}_j^T\dot{\boldsymbol{D}}\boldsymbol{\sigma}_j}{2} \\ =& \boldsymbol{\sigma}_j^T\Big[\boldsymbol{D}\left(\boldsymbol{\lambda}_P\dot{\boldsymbol{e}}_{Pj} + \boldsymbol{\lambda}_{F1}\dot{\boldsymbol{e}}_{Fj} + \boldsymbol{\lambda}_{F2}\ddot{\boldsymbol{e}}_F + \bar{\boldsymbol{S}}\ddot{\boldsymbol{P}}_d + \boldsymbol{S}\ddot{\boldsymbol{P}}_j\right) \\ & + \boldsymbol{C}\left(\dot{\boldsymbol{P}}_j + \boldsymbol{\sigma}_j\right) + \boldsymbol{G} - \left(\boldsymbol{J}_j^T\right)^{-1}\boldsymbol{\tau}_j + \boldsymbol{F}_{v,j} - \boldsymbol{F}_j\Big] \\ =& \boldsymbol{\sigma}_j^T\left(\boldsymbol{\Xi}^T\boldsymbol{\Psi}_j - \left(\boldsymbol{J}_j^T\right)^{-1}\boldsymbol{\tau}_j + \boldsymbol{F}_{v,j} - \boldsymbol{F}_j\right) \end{aligned} \tag{11}$$

where $\boldsymbol{\Xi} \in R^{3n\times n}$ and $\boldsymbol{\Psi}_j \in R^{3n\times 1}$ are an unknown time-varying matrix and a known vector function, respectively, and defined as

$$\begin{aligned} \boldsymbol{\Xi} &= \begin{bmatrix} \boldsymbol{D} & \boldsymbol{C} & \boldsymbol{G} \end{bmatrix}^T \\ \boldsymbol{\Psi}_j &= \begin{bmatrix} \boldsymbol{\lambda}_P\dot{\boldsymbol{e}}_{Pj} + \boldsymbol{\lambda}_{F1}\dot{\boldsymbol{e}}_{Fj} + \boldsymbol{\lambda}_{F2}\ddot{\boldsymbol{e}}_{Fj} + \bar{\boldsymbol{S}}\ddot{\boldsymbol{P}}_d + \boldsymbol{S}\ddot{\boldsymbol{P}}_j \\ \dot{\boldsymbol{P}}_j + \boldsymbol{\sigma}_j \\ \boldsymbol{1} \end{bmatrix} \end{aligned} \tag{12}$$

where $\boldsymbol{1}$ denotes an $n \times 1$ vector of ones.

Let $\boldsymbol{\Phi}_j^T\boldsymbol{\Theta} = \boldsymbol{\Xi}^T\boldsymbol{\Psi}_j$ where $\boldsymbol{\Theta} = \begin{bmatrix} \boldsymbol{\Xi}_1^T \cdots \boldsymbol{\Xi}_n^T \end{bmatrix}^T \in R^{3n^2\times 1}$ is an unknown vector which needs to be learned. $\boldsymbol{\Xi}_i$ with $i = 1, \ldots, n$ is the i-th column of $\boldsymbol{\Xi}$. In addition, the known matrix $\boldsymbol{\Phi}_j$ denotes a block diagonal matrix whose diagonal contains n blocks of $\boldsymbol{\Psi}_j$, i.e.

$$\boldsymbol{\Phi}_j = \begin{bmatrix} \boldsymbol{\Psi}_j & \cdots & \boldsymbol{0} \\ \vdots & \ddots & \vdots \\ \boldsymbol{0} & \cdots & \boldsymbol{\Psi}_j \end{bmatrix} \in R^{3n^2\times n}. \tag{13}$$

According to (11) and the sliding mode concept, the control law can be designed as

$$\begin{cases} \boldsymbol{\tau}_j = \boldsymbol{J}_j^T \left(\boldsymbol{k}\boldsymbol{\sigma}_j + \boldsymbol{\Phi}_j^T \hat{\boldsymbol{\Theta}}_j - \boldsymbol{F}_j + \hat{\alpha}_j \mathrm{sgn}\left(\boldsymbol{\sigma}_j\right) \right) \\ \hat{\boldsymbol{\Theta}}_j = \hat{\boldsymbol{\Theta}}_{j-1} + \boldsymbol{\Gamma}\boldsymbol{\Phi}_j\boldsymbol{\sigma}_j \\ \hat{\alpha}_j = \hat{\alpha}_{j-1} + \eta \boldsymbol{\sigma}_j^T \mathrm{sgn}\left(\boldsymbol{\sigma}_j\right) \end{cases} \tag{14}$$

where $\hat{\boldsymbol{\Theta}}_j$ and $\hat{\alpha}_j$ are the estimations of $\boldsymbol{\Theta}$ and α, $\hat{\boldsymbol{\Theta}}_{-1} = \boldsymbol{0}$, $\hat{\alpha}_{-1} = 0$ and $\boldsymbol{\Gamma}$ is a symmetric positive definite matrix, and sgn(•) denotes signum function.

3.2 Convergence analysis

Theorem 1 *Using the control law (14) for the nonlinear system (3),* $\lim\limits_{j\to\infty} \boldsymbol{e}_{P,j} = \boldsymbol{0}$ *and* $\lim\limits_{j\to\infty} \boldsymbol{e}_{F,j} = \boldsymbol{0}$.

Proof The proof can be divided into three parts. The first part is to redesign a Lyapunov function V_j and to prove that V_j is non-increasing in the iterative domain. The second part is to prove that V_0 is bounded. Finally, the convergence of $\boldsymbol{e}_P$ and $\boldsymbol{e}_F$ is proofed.

Redesign a Lyapunov function at j-th iteration as

$$V_j = V_{j1} + V_{j2} + V_{j3} \tag{15}$$

where $V_{j1} = \frac{\boldsymbol{\sigma}_j^T \boldsymbol{D}\boldsymbol{\sigma}_j}{2}$, $V_{j2} = \frac{1}{2}\int_0^t \tilde{\boldsymbol{\Theta}}_j^T \boldsymbol{\Gamma}^{-1} \tilde{\boldsymbol{\Theta}}_j \mathrm{d}\tau$ and $V_{j3} = \frac{1}{2\eta}\int_0^t \tilde{\alpha}_j^2 \mathrm{d}\tau$ with $\tilde{\boldsymbol{\Theta}}_j = \boldsymbol{\Theta} - \hat{\boldsymbol{\Theta}}_j$ and $\tilde{\alpha}_j = \alpha - \hat{\alpha}_j$. The non-increasing of V_j in the iterative domain is proven firstly.

The difference of V_{j1} is given by

$$\begin{aligned} \Delta V_{j1} =& \frac{\boldsymbol{\sigma}_j^T \boldsymbol{D}\boldsymbol{\sigma}_j}{2} - \frac{\boldsymbol{\sigma}_{j-1}^T \boldsymbol{D}\boldsymbol{\sigma}_{j-1}}{2} \\ =& \int_0^t \boldsymbol{\sigma}_j^T \left[\boldsymbol{\Phi}_j^T \boldsymbol{\Theta} - \left(\boldsymbol{J}^T\right)^{-1} \boldsymbol{\tau}_j - \boldsymbol{F}_j + \boldsymbol{F}_{v,j} \right] \mathrm{d}\tau \\ & - \frac{\boldsymbol{\sigma}_{j-1}^T \boldsymbol{D}\boldsymbol{\sigma}_{j-1}}{2} \\ =& \int_0^t \boldsymbol{\sigma}_j^T \left(\boldsymbol{\Phi}_j^T \boldsymbol{\Theta} + \boldsymbol{F}_{v,j} \right) \mathrm{d}\tau - \frac{\boldsymbol{\sigma}_{j-1}^T \boldsymbol{D}\boldsymbol{\sigma}_{j-1}}{2} \\ & - \int_0^t \boldsymbol{\sigma}_j^T \left[\boldsymbol{k}\boldsymbol{\sigma}_j + \boldsymbol{\Phi}_j^T \hat{\boldsymbol{\Theta}}_j + \hat{\boldsymbol{\Theta}}_j \mathrm{sgn}(\boldsymbol{\sigma}_j) \right] \mathrm{d}\tau. \end{aligned} \tag{16}$$

The difference of V_{j2} is given by

$$\begin{aligned} \Delta V_{j2} =& \frac{1}{2}\int_0^t \tilde{\boldsymbol{\Theta}}_j^T \boldsymbol{\Gamma}^{-1} \tilde{\boldsymbol{\Theta}}_j \mathrm{d}\tau \\ & - \frac{1}{2}\int_0^t \tilde{\boldsymbol{\Theta}}_{j-1}^T \boldsymbol{\Gamma}^{-1} \tilde{\boldsymbol{\Theta}}_{j-1} \mathrm{d}\tau \\ =& \frac{1}{2}\int_0^t -\left(\boldsymbol{\Gamma}\boldsymbol{\Phi}_j\boldsymbol{\sigma}_j\right)^T \boldsymbol{\Gamma}^{-1} \left(2\tilde{\boldsymbol{\Theta}}_j + \boldsymbol{\Gamma}\boldsymbol{\Phi}_j\boldsymbol{\sigma}_j \right) \mathrm{d}\tau \\ =& -\int_0^t \boldsymbol{\sigma}_j^T \boldsymbol{\Phi}^T \tilde{\boldsymbol{\Theta}}_j \mathrm{d}\tau - \frac{1}{2}\int_0^t \boldsymbol{\sigma}_j^T \boldsymbol{\Phi}_j^T \boldsymbol{\Gamma}\boldsymbol{\Phi}_j\boldsymbol{\sigma}_j \mathrm{d}\tau. \end{aligned} \tag{17}$$

The difference of V_{j3} is given by

$$\begin{aligned} \Delta V_{j3} =& \frac{1}{2\eta}\int_0^t \tilde{\alpha}_j^2 \mathrm{d}\tau - \frac{1}{2\eta}\int_0^t \tilde{\alpha}_{j-1}^2 \mathrm{d}\tau \\ =& \frac{1}{2\eta}\int_0^t -\eta\boldsymbol{\sigma}_j^T \mathrm{sgn}\left(\boldsymbol{\sigma}_j\right)\left(2\tilde{\alpha}_j + \eta\boldsymbol{\sigma}_j^T \mathrm{sgn}\left(\boldsymbol{\sigma}_j\right)\right) \mathrm{d}\tau \\ =& -\int_0^t \tilde{\alpha}_j \boldsymbol{\sigma}_j^T \mathrm{sgn}\left(\boldsymbol{\sigma}_j\right) \mathrm{d}\tau \\ & - \frac{\eta}{2}\int_0^t \left(\boldsymbol{\sigma}_j^T \mathrm{sgn}\left(\boldsymbol{\sigma}_j\right)\right)^2 \mathrm{d}\tau. \end{aligned} \tag{18}$$

Combining (15)-(18), yields

$$\begin{aligned} \Delta V_j =& \Delta V_{j1} + \Delta V_{j2} + \Delta V_{j3} \\ =& \int_0^t \boldsymbol{\sigma}_j^T \left(\boldsymbol{\Phi}_j^T \boldsymbol{\Theta} + \boldsymbol{F}_{v,j} \right) \mathrm{d}\tau - \frac{\boldsymbol{\sigma}_{j-1}^T \boldsymbol{D}\boldsymbol{\sigma}_{j-1}}{2} \\ & - \int_0^t \boldsymbol{\sigma}_j^T \left[\boldsymbol{k}\boldsymbol{\sigma}_j + \boldsymbol{\Phi}_j^T \hat{\boldsymbol{\Theta}}_j + \hat{\boldsymbol{\Theta}}_j \mathrm{sgn}(\boldsymbol{\sigma}_j) \right] \mathrm{d}\tau \\ & - \int_0^t \boldsymbol{\sigma}_j^T \boldsymbol{\Phi}^T \tilde{\boldsymbol{\Theta}}_j \mathrm{d}\tau - \frac{1}{2}\int_0^t \boldsymbol{\sigma}_j^T \boldsymbol{\Phi}_j^T \boldsymbol{\Gamma}\boldsymbol{\Phi}_j\boldsymbol{\sigma}_j \mathrm{d}\tau \\ & - \int_0^t \tilde{\boldsymbol{\Theta}}_j \boldsymbol{\sigma}_j^T \mathrm{sgn}\left(\boldsymbol{\sigma}_j\right) \mathrm{d}\tau \\ & - \frac{\eta}{2}\int_0^t \left(\boldsymbol{\sigma}_j^T \mathrm{sgn}\left(\boldsymbol{\sigma}_j\right)\right)^2 \mathrm{d}\tau \\ =& -\int_0^t \boldsymbol{\sigma}_j^T \boldsymbol{k}\boldsymbol{\sigma}_j \mathrm{d}\tau - \frac{1}{2}\int_0^t \boldsymbol{\sigma}_j^T \boldsymbol{\Phi}_j^T \boldsymbol{\Gamma}\boldsymbol{\Phi}_j\boldsymbol{\sigma}_j \mathrm{d}\tau \\ & - \frac{\eta}{2}\int_0^t \left(\boldsymbol{\sigma}_j^T \mathrm{sgn}\left(\boldsymbol{\sigma}_j\right)\right)^2 \mathrm{d}\tau - \frac{\boldsymbol{\sigma}_{j-1}^T \boldsymbol{D}\boldsymbol{\sigma}_{j-1}}{2} \\ & - \int_0^t \alpha_j \boldsymbol{\sigma}_j^T \mathrm{sgn}\left(\boldsymbol{\sigma}_j\right) \mathrm{d}\tau - \int_0^t \boldsymbol{\sigma}_j^T \boldsymbol{F}_{v,j} \mathrm{d}\tau \\ \leq& -\int_0^t \left(\alpha_j - \|\boldsymbol{F}_{v,j}\|\right) \|\boldsymbol{\sigma}_j\| \mathrm{d}\tau \\ \leq& 0. \end{aligned} \tag{19}$$

Since $\alpha_j \geq \|\boldsymbol{F}_{v,j}\|$, $\Delta V_j \leq 0$ such that V_j is non-increasing.

Then, we prove that $V_j(t)$ is bounded over $t \in [0,\, T]$. Taking the time derivative of V_0, yields

$$\begin{aligned} \dot{V}_0 =& \boldsymbol{\sigma}_0^T \left[\boldsymbol{\Phi}_0^T \boldsymbol{\Theta}_0 - \left(\boldsymbol{k}\boldsymbol{\sigma}_0 + \boldsymbol{\Phi}_0^T \hat{\boldsymbol{\Theta}} + \hat{\alpha}_0 \mathrm{sgn}(\boldsymbol{\sigma}_0) \right) + \boldsymbol{F}_{v,0} \right] \\ & + \frac{1}{2}\tilde{\boldsymbol{\Theta}}_0^T \boldsymbol{\Gamma}^{-1} \tilde{\boldsymbol{\Theta}}_0 + \frac{\tilde{\alpha}_0^2}{2\eta} \\ =& \boldsymbol{\sigma}_0^T \left[\boldsymbol{\Phi}_0^T \tilde{\boldsymbol{\Theta}}_0 + \tilde{\alpha}_0 \mathrm{sgn}(\boldsymbol{\sigma}_0) - \boldsymbol{k}\boldsymbol{\sigma}_0 - \alpha_0 \mathrm{sgn}(\boldsymbol{\sigma}_0) + \boldsymbol{F}_{v,0} \right] \\ & + \frac{1}{2}\tilde{\boldsymbol{\Theta}}_0^T \boldsymbol{\Gamma}^{-1} \tilde{\boldsymbol{\Theta}}_0 + \frac{\tilde{\alpha}_0^2}{2\eta}. \end{aligned} \tag{20}$$

Since $\hat{\boldsymbol{\Theta}}_{-1} = \boldsymbol{0}$ and $\hat{\alpha}_{-1} = 0$, we can obtain $\hat{\boldsymbol{\Theta}}_0 = \boldsymbol{\Gamma}\boldsymbol{\Phi}_0\boldsymbol{\sigma}_0$ and $\hat{\alpha}_0 = \eta\boldsymbol{\sigma}_0^T \mathrm{sgn}\left(\boldsymbol{\sigma}_0\right)$. Then, (20) can be rear-

ranged as

$$\begin{aligned}\dot{V}_0 =& -\boldsymbol{\sigma}_0^T \boldsymbol{k}\boldsymbol{\sigma}_0 - \boldsymbol{\sigma}_0^T(\alpha \mathrm{sgn}(\boldsymbol{\sigma}_0) - \boldsymbol{F}_{v,0}) \\ & - \frac{1}{2}\tilde{\boldsymbol{\Theta}}_0^T \boldsymbol{\Gamma}^{-1}\tilde{\boldsymbol{\Theta}}_0 + \boldsymbol{\Theta}^T\boldsymbol{\Gamma}^{-1}\tilde{\boldsymbol{\Theta}}_0 - \frac{\tilde{\alpha}_0^2}{2\eta} + \frac{1}{\eta}\tilde{\alpha}_0\alpha.\end{aligned} \tag{21}$$

According to the Young's inequality [37], we have

$$\begin{aligned}&\boldsymbol{\Theta}^T\boldsymbol{\Gamma}^{-1}\tilde{\boldsymbol{\Theta}}_0 \le \frac{\chi_1}{2}\left\|\boldsymbol{\Gamma}^{-1}\tilde{\boldsymbol{\Theta}}_0\right\|^2 + \frac{1}{2\chi_1}\|\boldsymbol{\Theta}\|^2, \ \forall \chi_1 > 0 \\ &\frac{1}{\eta}\tilde{\alpha}_0\alpha \le \frac{\chi_2}{2}\frac{\tilde{\alpha}_0^2}{\eta^2} + \frac{\alpha^2}{2\chi_2}, \qquad \forall \chi_2 > 0.\end{aligned} \tag{22}$$

Substituting (22) into (21), yields

$$\begin{aligned}\dot{V}_0 \le & -\lambda_{\min}(\boldsymbol{k})\|\boldsymbol{\sigma}_0\|^2 - (\alpha - \|\boldsymbol{F}_{v,0}\|)\|\boldsymbol{\sigma}_0\| \\ & - \left(\frac{1}{2}\lambda_{\min}(\boldsymbol{\Gamma}^{-1}) - \frac{\chi_1}{2}\lambda_{\max}^2(\boldsymbol{\Gamma}^{-1})\right)\left\|\tilde{\boldsymbol{\Theta}}_0\right\|^2 \\ & - \left(1 - \frac{\chi_2}{\eta}\right)\frac{\tilde{\alpha}_0^2}{2\eta} + \frac{1}{2\chi_1}\|\boldsymbol{\Theta}\|^2 + \frac{\alpha^2}{2\chi_2}\end{aligned} \tag{23}$$

where $\lambda_{\min}(\bullet)$ and $\lambda_{\max}(\bullet)$ denote the minimal and maximal eigenvalue of matrix $\bullet$. When $0 < \chi_1 \le \frac{\lambda_{\min}(\boldsymbol{\Gamma}^{-1})}{\lambda_{\max}^2(\boldsymbol{\Gamma}^{-1})}$ and $0 < \chi_2 \le \eta$, we have

$$\dot{V}_0 \le \frac{1}{2\chi_1}\|\boldsymbol{\Theta}\|^2 + \frac{\alpha^2}{2\chi_2}. \tag{24}$$

Since $\boldsymbol{\Theta}$ and α are bounded over $t \in [0, T]$, $\dot{V}_0$ is bounded over $t \in [0, T]$. Then, V_0 is bounded over $t \in [0, T]$.

Finally, combining (15) and (19), yields

$$\lim_{j\to\infty} \boldsymbol{\sigma}_j = \boldsymbol{0}. \tag{25}$$

Since $\boldsymbol{S}$ and $\bar{\boldsymbol{S}}$ are complementary, $\boldsymbol{\sigma}_P$ and $\boldsymbol{\sigma}_F$ are orthogonal. Therefore, $\lim_{j\to\infty} \boldsymbol{\sigma}_{P,j} = \boldsymbol{0}$ and $\lim_{j\to\infty} \boldsymbol{\sigma}_{F,j} = \boldsymbol{0}$. Then we can obtain that $\lim_{j\to\infty} \boldsymbol{e}_{P,j} = \boldsymbol{0}$ and $\lim_{j\to\infty} \boldsymbol{e}_{F,j} = \boldsymbol{0}$.

4 Simulation Studies

4.1 System description

Simulation studies are performed on a 2-DOFs planar parallel manipulator depicted in Fig. 1. The manipulator has 5 revolute joints, including 2 actuated joints and 3 passive joints. In the simulation studies, the contact surface is given as $y_e = 0.4$m. θ_1 and θ_2 are the actuated joints. Suppose that the stiffness of the environment is $K_e = 1000$N/m and the initial position of the manipulator is on the contact surface. The parameters of the manipulator are given as Table 1. L_i, L_{ci}, m_i and I_i denote the length, length from head to center of mass, mass, and the inertial around the center of mass of link i, respectively.

Table 1 The parameters of the manipulator

Parameters	Values	Units
L_1	0.2794	m
L_2	0.2794	m
L_3	0.3048	m
L_4	0.3048	m
L_5	0.3048	m
L_{c1}	0.1466	m
L_{c2}	0.1410	m
L_{c3}	0.1581	m
L_{c4}	0.1467	m
m_1	0.2451	kg
m_2	0.2352	kg
m_3	0.2611	kg
m_4	0.2611	kg
I_1	2.779×10^{-3}	kg · m^2
I_2	2.607×10^{-3}	kg · m^2
I_3	3.476×10^{-3}	kg · m^2
I_4	3.476×10^{-3}	kg · m^2

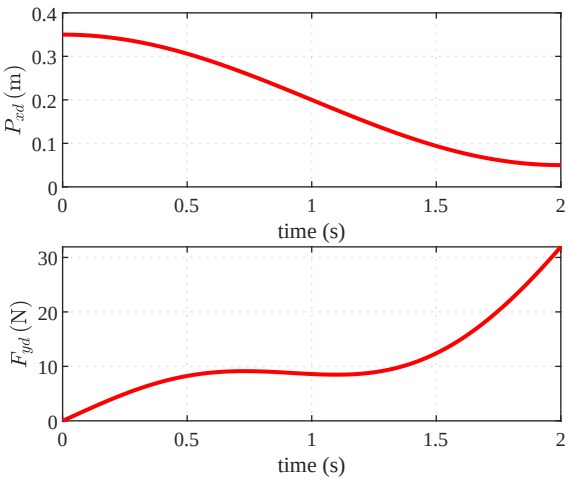

Fig. 2 The desired position and desired force

In the simulation studies, assume that the position control is conducted in the X direction and the force control is conducted in the Y direction. Therefore, $\boldsymbol{S} = \mathrm{diag}([1, 0])$.

The desired position in the X direction is given as $P_{xd} = 0.15\cos(\pi t/2) + 0.2$ and the desired force in the Y direction is given as $F_{yd} = 5\sin(\pi t) + 5(e^t - 1)$ over the time interval [0, 2s]. The desired position and desired force are shown in Fig. 2. To demonstrate the robustness of the proposed method against parameter perturbation, m_3 , the mass of link 3, is changed to 1.4 times from iteration $j = 10$.

The controller parameters are designed as $\boldsymbol{\lambda}_P = \mathrm{diag}([2, 0])$, $\boldsymbol{\lambda}_{F1} = \mathrm{diag}([0, 10^{-3}])$, $\boldsymbol{\lambda}_{F2} = \mathrm{diag}([0, 10^{-4}])$, $\boldsymbol{\Gamma} = \mathrm{diag}([4\times10^3, 40, 10^4, 10^4, 10^3, 10^3, 10^4, 10^4])$, $\boldsymbol{k} = \mathrm{diag}([10, 100])$ and $\eta = 5$.

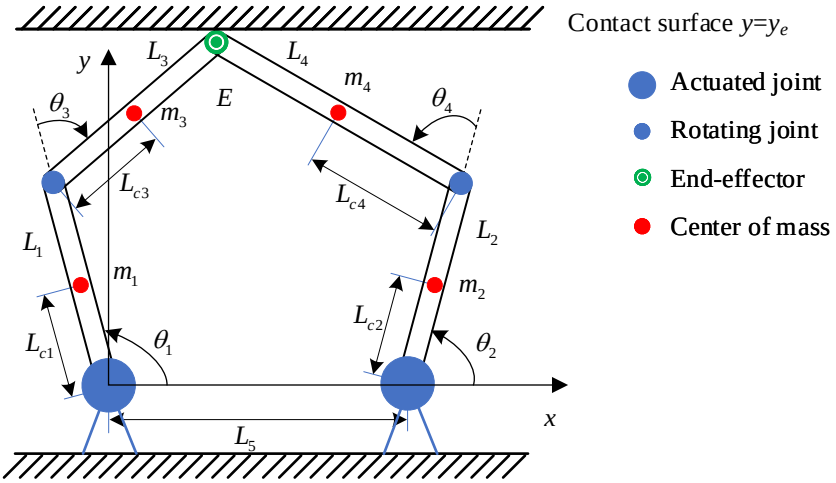

Fig. 1 A 2-DOFs planar parallel manipulator

To demonstrate the effectiveness of the proposed method, performance comparisons are conducted among the following three methods:

C1: Traditional SMC. The control law is designed as

$$\boldsymbol{\tau}_j = \boldsymbol{J}^T \left(\boldsymbol{k}\boldsymbol{\sigma}_j + \alpha \mathrm{sgn}(\boldsymbol{\sigma}_j) + \boldsymbol{\Xi}^T \boldsymbol{\Psi}_j - \boldsymbol{F}_j \right) \tag{26}$$

where $\boldsymbol{\Xi}$, containing the dynamics information, is calculated by using a nominal model, the switching gain $\alpha = 0.1$ and the control gain $\boldsymbol{k} = \mathrm{diag}([10,\ 100])$. The other control parameters of the traditional SMC are the same as the proposed method.

C2: Traditional ILC. The control law is designed as [38]

$$\begin{aligned} \boldsymbol{\tau}_j &= \boldsymbol{v}_j - \boldsymbol{J}_j^T \boldsymbol{F}_j \\ \boldsymbol{v}_j &= \boldsymbol{v}_{j-1} + \boldsymbol{J}_j^T \boldsymbol{k}\boldsymbol{\sigma}_j \end{aligned} \tag{27}$$

where $\boldsymbol{k} = \mathrm{diag}([400,\ 400])$. In this control law, $\boldsymbol{v}_j$ is the learned part and $\boldsymbol{J}_j^T \boldsymbol{F}_j$ is the joint torque corresponding to the output force of end-effector.

C3: The proposed method.

4.2 Simulation results

4.2.1 Tracking performance

The 2-norms of the position tracking error and force tracking error are depicted in Figs. 3 and 4, respectively. Firstly, the data before $j = 10$ in those figures are compared. Obviously, it can be noticed that C_2 and C_3 achieve better tracking performance than C_1. Let $\bar{j}$ denote the iteration when the tracking error converges. Then, $\bar{j}$ and the 2-norms of the corresponding tracking error $\|e_{P,\bar{j}}\|_2$ and $\|e_{F,\bar{j}}\|_2$ of C_2 and C_3 before adding

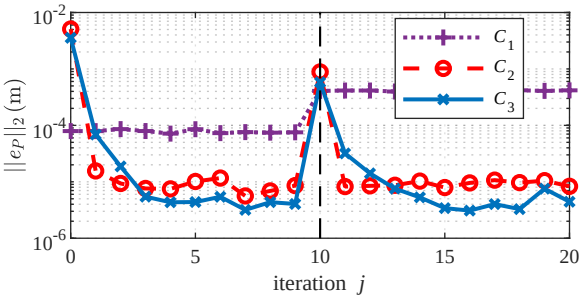

Fig. 3 The 2-norm of the position tracking error

the system parameter perturbation are detailed in Table 2. The convergent speed of C_3 is slightly slower than that of C_2 but the 2-norm of the tracking error of C_3 is reduced more than 40% compared with that of C_2. Additionally, C_3 attains better tracking performance than C_2 after tracking error convergence in the presence of non-repetitive disturbances since C_2 is incapable of learning non-repetitive disturbances while the sliding mode term in C_3 can deal with it. When the system parameter perturbation is added at iteration $j = 10$, the 2-norms of C_2 and C_3 are significantly deteriorated while that of C_1 is slightly worse. However, the tracking error of C_2 and C_3 is convergent again as the iteration continues. The comparison of the tracking performance of the three methods is also observed from Fig. 5 which shows the tracking error of the position (in the X direction) and force (in the Y direction) at iteration $j = 0, 5, 10, 15$.

4.2.2 Chattering suppression of control input

To evaluate the chattering effect of control input, a variable H is defined. H is the standard deviation of $\Delta\boldsymbol{\tau} = \boldsymbol{\tau}_d - \boldsymbol{\tau}$ where $\boldsymbol{\tau}_d$ is the desired control input. $\boldsymbol{\tau}_d$

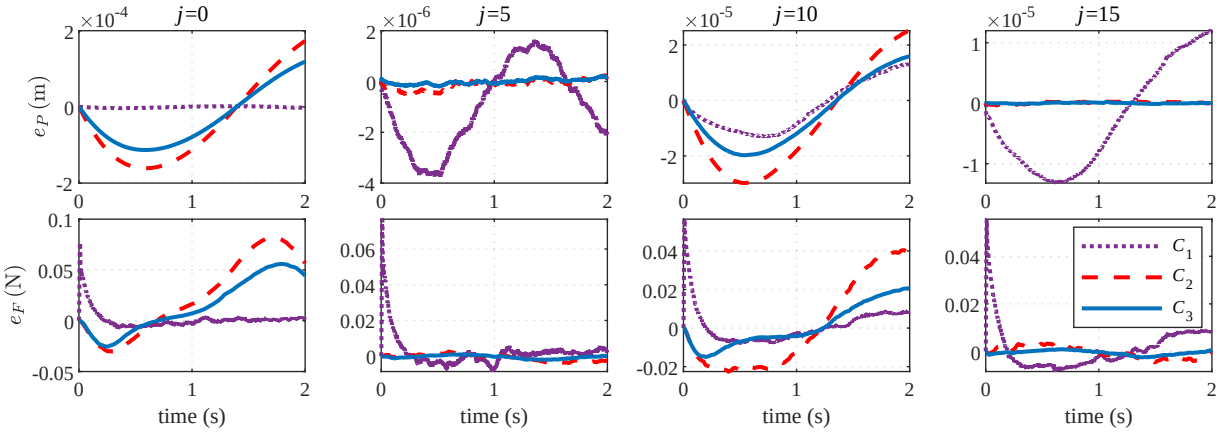

Fig. 5 Tracking error with $j = 0, 5, 10, 15$

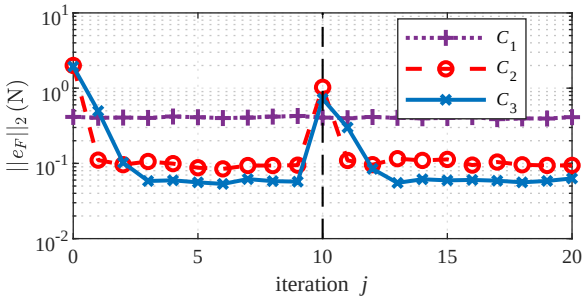

Fig. 4 The 2-norm of the force tracking error

Table 2 The iterations and 2-norms of the corresponding tracking error

Method	Position (X direction)		Force (Y direction)	
	$\bar{j}$	$\|e_{P,\bar{j}}\|_2$	$\bar{j}$	$\|e_{F,\bar{j}}\|_2$
C_2	3	7.6×10^{-6}	2	0.096
C_3	4	4.3×10^{-6}	3	0.058

can be calculated by (1) according to the desired trajectory. H of C_1 and C_3 at iteration $j = 20$ are listed in Table 3. It can be seen that H of C_1 is 1.67 times in the X direction and 2.44 times in the Y direction compared with H of C_3. Therefore, C_3 can effectively suppress the chattering of control input than C_1. This observation is confirmed by Figs. 6 and 7. Fig. 6 shows the control input and $\Delta\boldsymbol{\tau}$ of C_1 and C_3 in the X direction at iteration $j = 20$, and Fig. 7 shows the control input and $\Delta\boldsymbol{\tau}$ of C_1 and C_3 in the Y direction at iteration $j = 20$. Actually, H of C_1 can be reduced by reducing the switching gain of the sliding mode term. However, the tracking performance of C_1 will deteriorate at the same time. In C_3, the switching gain of the sliding mode term is time-varying and obtained by ILC, therefore, the chattering of control input is suppressed effectively while achieving better tracking performance than C_1.

Table 3 H of C_1 and C_3

	X direction	Y direction
C_1	0.06	0.0534
C_3	0.0359	0.0219

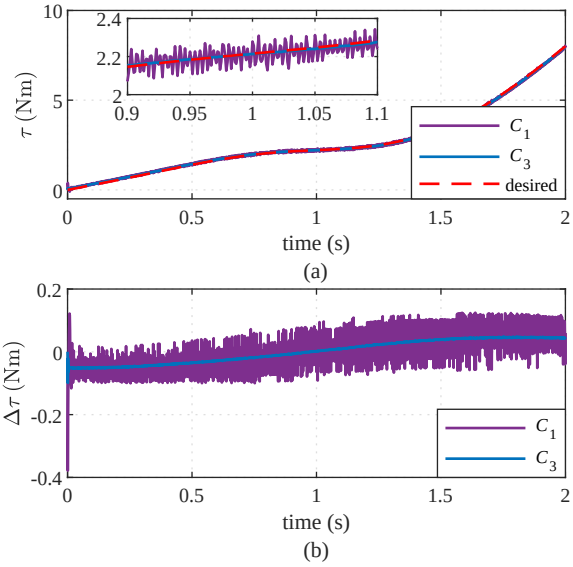

Fig. 6 (a) The control input in the X direction. (b) $\Delta\boldsymbol{\tau}$ in the X direction

5 Conclusion

Hybrid force/position control for robot manipulators has become a hot spot in recent years. In this paper, an ILC method based on sliding mode technique has been proposed to realize superior tracking performance for repetitive hybrid force/position control tasks of robot manipulators. Compared to the traditional SMC and ILC, the proposed method exhibits the following advantages: (i) It significantly improves the force/position tracking performance than traditional SMC. (ii) Com-

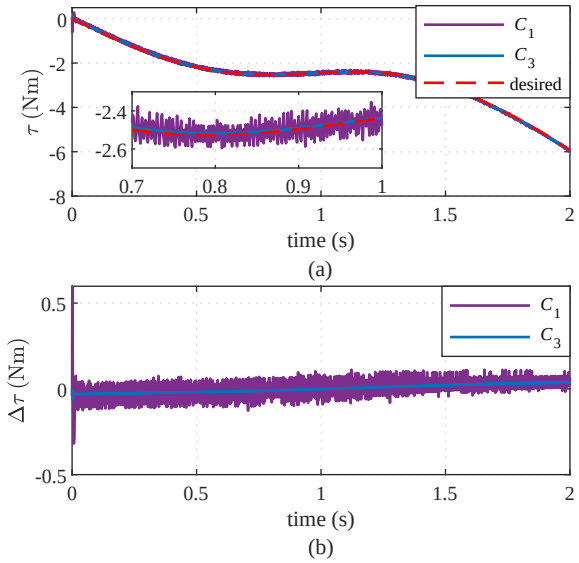

Fig. 7 (a) The control input in the Y direction. (b) $\Delta\boldsymbol{\tau}$ in the Y direction

pared with traditional ILC, it has stronger robustness against external disturbances and noise. (iii) Since the switching gain of the sliding mode term is variable and updated by ILC, the chattering of the control input is significantly suppressed compared with traditional SMC. The simulation results demonstrate the effectiveness of the proposed method.

Funding This work was supported in part by Major Project of Hubei Province Technology Innovation under grant 2019AAA071, the National Natural Science Foundation of China under Grant 51805496.

Declarations

Conflict of interest The authors declare that they have no conflict of interest.

Data availability statements The data that support the findings of this study are available from the author [X. Zhang], upon reasonable request.

References

1. M. Fazeli, M.J. Sadigh, in *2012 IEEE International Conference on Cyber Technology in Automation, Control, and Intelligent Systems (CYBER)* (2012), pp. 297–302
2. X. Xu, W. Chen, D. Zhu, S. Yan, H. Ding, Hybrid active/passive force control strategy for grinding marks suppression and profile accuracy enhancement in robotic belt grinding of turbine blade, Robotics and Computer-Integrated Manufacturing **67**, 102047 (2021)
3. J. Norberto Pires, G. Afonso, N. Estrela, Force control experiments for industrial applications: A test case using an industrial deburring example, Assembly Automation **27**(2), 148 (2007)
4. Y.L. Kuo, S.Y. Huang, C.C. Lan, in *2019 International Conference on Robotics and Automation (ICRA)* (IEEE, 2019), pp. 9489–9495
5. J.E. Solanes, L. Gracia, P. Muñoz-Benavent, J. Valls Miro, C. Perez-Vidal, J. Tornero, Robust hybrid position-force control for robotic surface polishing, Journal of Manufacturing Science and Engineering **141**(1) (2019)
6. M.T. Mason, Compliance and force control for computer controlled manipulators, IEEE Transactions on Systems, Man, and Cybernetics **11**(6), 418 (1981)
7. M. Reibert, J. Craig, Hybrid position/force control of manipulators, Journal of Dynamic Systems, Measurement, and Control **102**, 126 (1981)
8. L. Kuang-Yow, L. Chia-Ru, Sliding-mode motion/force control of constrained robots, IEEE Transactions on Automatic Control **43**(8), 1101 (1998)
9. D. Xiao, B. Ghosh, N. Xi, T. Tarn, Sensor-based hybrid position/force control of a robot manipulator in an uncalibrated environment, IEEE Transactions on Control Systems Technology **8**(4), 635 (2000)
10. M. Madani, M. Moallem, Hybrid position/force control of a flexible parallel manipulator, Journal of the Franklin Institute **348**(6), 999 (2011)
11. J. Cazalilla, M. Vallés, Á. Valera, V. Mata, M. Díaz-Rodríguez, Hybrid force/position control for a 3-DOF 1T2R parallel robot: Implementation, simulations and experiments, Mechanics Based Design of Structures and Machines **44**(1-2), 16 (2016)
12. J. Lin, T.S. Chiang, in *Proceedings of the 2003 American Control Conference, 2003.*, vol. 6 (2003), vol. 6, pp. 5239–5244 vol.6
13. M.S. Ju, C.C. Lin, D.H. Lin, I.S. Hwang, S.M. Chen, A rehabilitation robot with force-position hybrid fuzzy controller: Hybrid fuzzy control of rehabilitation robot, IEEE Transactions on Neural Systems and Rehabilitation Engineering **13**(3), 349 (2005)
14. L. Vladareanu, V. Vladareanu, P. Schiopu, Hybrid Force-Position Dynamic Control of the Robots Using Fuzzy Applications, Applied Mechanics and Materials **245**, 15 (2013)
15. Y. Li, G. Wang, B. Dong, B. Zhao, Hybrid position–force control for constrained reconfig-

urable manipulators based on adaptive neural network, Advances in Mechanical Engineering **7**(9), 1687814015602409 (2015)
16. N. Kumar, V. Panwar, N. Sukavanam, S.P. Sharma, J.H. Borm, Neural network based hybrid force/position control for robot manipulators, International Journal of Precision Engineering and Manufacturing **12**(3), 419 (2011)
17. C. Cao, F. Wang, Q. Cao, H. Sun, W. Xu, M. Cui, Neural network–based terminal sliding mode applied to position/force adaptive control for constrained robotic manipulators, Advances in Mechanical Engineering **10**(6), 1 (2018)
18. M.H. Ghajar, M. Keshmiri, J. Bahrami, Neural-network-based robust hybrid force/position controller for a constrained robot manipulator with uncertainties, Transactions of the Institute of Measurement and Control **40**(5), 1625 (2018)
19. H. Kawasaki, S. Ueki, S. Ito, Decentralized adaptive coordinated control of multiple robot arms without using a force sensor, Automatica **42**(3), 481 (2006)
20. S.A.M. Dehghan, M. Danesh, F. Sheikholeslam, Adaptive hybrid force/position control of robot manipulators using an adaptive force estimator in the presence of parametric uncertainty, Advanced Robotics **29**(4), 209 (2015)
21. D.M. Tuan, P.D. Hieu, Adaptive Position/Force Control for Robot Manipulators Using Force and Velocity Observer, Journal of Electrical Engineering & Technology **14**(6), 2575 (2019)
22. A.C. Leite, F.L. Cruz, F. Lizarralde, Adaptive Passivity-based Hybrid Pose/Force Control for Uncertain Robots, IFAC-PapersOnLine **53**(2), 3854 (2020)
23. A. Karamali Ravandi, E. Khanmirza, K. Daneshjou, Hybrid force/position control of robotic arms manipulating in uncertain environments based on adaptive fuzzy sliding mode control, Applied Soft Computing **70**, 864 (2018)
24. H. Navvabi, A.H.D. Markazi, Hybrid position/force control of Stewart Manipulator using Extended Adaptive Fuzzy Sliding Mode Controller (E-AFSMC), ISA Transactions **88**, 280 (2019)
25. H. Chaudhary, V. Panwar, R. Prasad, N. Sukavanam, Adaptive neuro fuzzy based hybrid force/position control for an industrial robot manipulator, Journal of Intelligent Manufacturing **27**(6), 1299 (2016)
26. S. Arimoto, S. Kawamura, F. Miyazaki, Bettering operation of Robots by learning, Journal of Robotic Systems **1**(2), 123 (1984)
27. T. Lin, D.H. Owens, J. Hätönen, Newton method based iterative learning control for discrete nonlinear systems, International Journal of Control **79**(10), 1263 (2006)
28. D.H. Owens, S. Liu, Iterative learning control: Quantifying the effect of output noise, IET Control Theory Applications **5**(2), 379 (2011)
29. X. Zhang, M. Li, H. Ding, X. Yao, Data-driven tuning of feedforward controller structured with infinite impulse response filter via iterative learning control, IET Control Theory & Applications **13**(8), 1062 (2019)
30. D.A. Bristow, M. Tharayil, A.G. Alleyne, A survey of iterative learning control, IEEE Control Systems **26**(3), 96 (2006)
31. H.S. Ahn, Y. Chen, K.L. Moore, Iterative Learning Control: Brief Survey and Categorization, IEEE Transactions on Systems, Man, and Cybernetics, Part C (Applications and Reviews) **37**(6), 1099 (2007)
32. J.X. Xu, A survey on iterative learning control for nonlinear systems, International Journal of Control **84**(7), 1275 (2011)
33. W. Xu, Robotic Time-Varying Force Tracking in Position-Based Impedance Control, Journal of Dynamic Systems, Measurement, and Control **138**(9) (2016)
34. H. Parzer, H. Gattringer, A. Müller, R. Naderer, in *Advances in Robot Design and Intelligent Control* (Cham, 2017), Advances in Intelligent Systems and Computing, pp. 12–19
35. L. Roveda, G. Pallucca, N. Pedrocchi, F. Braghin, L.M. Tosatti, Iterative Learning Procedure With Reinforcement for High-Accuracy Force Tracking in Robotized Tasks, IEEE Transactions on Industrial Informatics **14**(4), 1753 (2018)
36. M.W. Spong, S. Hutchinson, M. Vidyasagar, *Robot Modeling and Control*, second edition edn. (Hoboken, NJ, 2020)
37. H. Jarchow, *Locally Convex Spaces*. Mathematische Leitfäden (Stuttgart, 1981)
38. A. Azenha, Iterative learning in variable structure position/force hybrid control of manipulators, Robotica **18**(2), 213 (2000)